Journal of Membrane Science 568 (2018) 113–120

Contents lists available at ScienceDirect

Journal of Membrane Science

journal homepage: www.elsevier.com/locate/memsci

Hydrogen production via natural gas steam reforming in a Pd-Au membrane reactor. Comparison between methane and natural gas steam reforming reactions

Bryce Anzelmo[a], Jennifer Wilcox[a,b], Simona Liguori[a,b,*]

[a] Department of Energy Resources Engineering, Stanford University, 367 Panama St., Stanford, CA 94305, United States
[b] Chemical and Biological Engineering Department, Colorado School of Mines, Golden, CO 80401, United States

ARTICLE INFO

Keywords:
Hydrogen
Natural gas reforming
Palladium-gold
Composite membrane
Membrane reactor

ABSTRACT

High-purity hydrogen to be fed directly to a PEMFC was produced by carrying out natural gas steam reforming under moderate operating conditions in a Pd-Au composite membrane reactor packed with a commercial Ni-based catalyst. The Pd-Au composite membrane with a thickness of approximately 12 μm was fabricated by using both electroless and electroplating techniques to deposit Pd and Au layers, respectively, over a porous stainless-steel support. After annealing, the membrane showed a hydrogen permeance of 1.30×10^{-3} mol/s-m^2-Pa$^{0.5}$ at 450 °C, and near-infinite ideal selectivity of H2/Ar at pressures lower than 300 kPa and at temperatures lower than 400 °C. The natural gas reforming reaction was performed at 450 °C with a steam-to-methane ratio of 3.5 and gas hourly space velocity of 2600 h^{-1} at different operating pressures varying from 100 kPa to 300 kPa. As a comparison, the steam methane reforming reaction was also carried out at the same operating conditions.

The natural gas reforming reaction showed better performance than the steam methane reforming reaction and reached > 80% conversion of the higher hydrocarbons and almost 65% of hydrogen recovery at 450 °C and 300 kPa. High-purity hydrogen was obtained in all the experimental tests. No coke formation was observed. Post-reaction analysis of the membrane is discussed via scanning electron microscope and energy-dispersive X-ray spectroscopy.

1. Introduction

Over the past decade, there has been an increase in the application of hydrogen as an energy vector due to its environmentally friendly quality and wide range of energy applications [1]. Currently, close to 50% of the hydrogen global demand is produced via steam reforming of natural gas [2], which is the most economic technology among all hydrogen production pathways [3]. Although natural gas (NG) consists mostly of methane, its composition can vary widely depending on the geologic reservoir from which it is recovered. Well location, geological conditions, and extraction method can dictate the level of impurities, e.g., water, nitrogen, hydrogen sulfide and higher-order hydrocarbons, contained within the natural gas. Once *raw* natural gas is processed (e.g., sulfur removal, etc.), it can enter the pipeline distribution system followed by consumption of the end-use product. The NG consumed in the U.S. has a standard heating value of approximately 1000 BTU/ft^3 (1000 kJ/28 L) at STP [4]. Hence, given that the standardization is based on the heating value rather than the gas composition, a compositional range of gases, largely determined from a safety perspective by the Pipeline and Hazardous Materials Safety Administration sector of the U.S. Department of Transportation, can be found within NG [5]. The maximum compositional limit for various components of pipeline-quality NG [6–9] is shown in Table 1.

Currently, the conversion of NG to hydrogen takes place in a conventional reformer at harsh operating conditions. The general reaction describing NG steam reforming (SR) can be described as [10]:

$$C_xH_y + xH_2O \leftrightarrow \left(x + \frac{y}{2}\right)H_2 + xCO \quad (1)$$

where x is the number of carbon atoms and y is the number of hydrogen atoms within the hydrocarbon feed. For example, if the feed is methane, as described previously, Eq. 1 reduces into Eq. (2). Furthermore, the three main reactions governing the steam methane reforming (SMR) process are [11]:

$$CH_4 + H_2O \leftrightarrow CO + 3H_2 \quad \Delta H^{\circ}_{298K} = 206 \text{ kJ/mol} \quad (2)$$

* Corresponding author at: Department of Energy Resources Engineering, Stanford University, 367 Panama St., Stanford, CA 94305, United States.
E-mail address: sliguori@mines.edu (S. Liguori).

https://doi.org/10.1016/j.memsci.2018.09.054
Received 11 May 2018; Received in revised form 9 September 2018; Accepted 23 September 2018
Available online 26 September 2018
0376-7388/

Table 1
Maximum composition limits of various components for pipeline quality natural gas.

Component	Maximum [mol%]
Methane	> 96
Ethane	10
Propane	5
Butane	2
Nitrogen	4
Carbon Dioxide	4

$$CO + H_2O \leftrightarrow CO_2 + H_2 \quad \Delta H^{\circ}_{298K} = -41\ \text{kJ/mol} \tag{3}$$

$$CH_4 + 2H_2O \leftrightarrow CO_2 + 4H_2 \quad \Delta H^{\circ}_{298K} = 165\ \text{kJ/mol} \tag{4}$$

However, NG contains several other hydrocarbons (HCs) as shown in Table 1, that react across the same catalytic bed, typically comprised of Ni, thereby leading to additional reactions [12]. Therefore, for SR of ethane, the following reactions are known to be prevalent [13]:

$$C_2H_6 + 2H_2O \leftrightarrow 2CO + 5H_2 \quad \Delta H^{\circ}_{298K} = 346\ \text{kJ/mol} \tag{5}$$

$$C_2H_6 + H_2 \leftrightarrow 2CH_4 \quad \Delta H^{\circ}_{298K} = -66\ \text{kJ/mol} \tag{6}$$

$$CO + 3H_2 \leftrightarrow CH_4 + H_2O \quad \Delta H^{\circ}_{298K} = -206\ \text{kJ/mol} \tag{7}$$

$$2CO + 2H_2O \leftrightarrow 2CO_2 + 2H_2 \quad \Delta H^{\circ}_{298K} = -82\ \text{kJ/mol} \tag{8}$$

$$C_2H_6 + 4H_2O \leftrightarrow 2CO_2 + 7H_2 \quad \Delta H^{\circ}_{298K} = 264\ \text{kJ/mol} \tag{9}$$

Similarly, the dominant pathways for SR of propane are [14]:

$$C_3H_8 + 3H_2O \leftrightarrow 3CO + 7H_2 \quad \Delta H^{\circ}_{298K} = 499\ \text{kJ/mol} \tag{10}$$

$$C_3H_8 + 6H_2O \leftrightarrow 3CO_2 + 10H_2 \quad \Delta H^{\circ}_{298K} = 375\ \text{kJ/mol} \tag{11}$$

Also, the pathways for SR of butane [15] are:

$$CO_2 + 4H_2 \leftrightarrow CH_4 + 2H_2O \quad \Delta H^{\circ}_{298K} = -165\ \text{kJ/mol} \tag{12}$$

$$C_4H_{10} + 3H_2 \leftrightarrow 4CH_4 \quad \Delta H^{\circ}_{298K} = -174\ \text{kJ/mol} \tag{13}$$

$$C_4H_{10} + 4H_2O \leftrightarrow 4CO + 9H_2 \quad \Delta H^{\circ}_{298K} = 650\ \text{kJ/mol} \tag{14}$$

$$C_4H_{10} + 8H_2O \leftrightarrow 4CO_2 + 13H_2 \quad \Delta H^{\circ}_{298K} = 486\ \text{kJ/mol} \tag{15}$$

Additionally, a complex network of side reactions can take place to form various HC species. Comprehensive literature studies relating to the industrial process of NG reforming are available in terms of catalyst deactivation, kinetics, energy evaluation, life cycle analysis, among other parameters [16–19].

The industrial reformed stream contains mainly H_2 and by-products such as CO_2 and CO. In order to obtain pure hydrogen, the industrial reformer is followed by water gas shift (WGS) reactors and equipment for hydrogen separation and purification. In the context of process intensification, the membrane reactor (MR) can be used to perform SR reactions and remove pure hydrogen within the same device. In particular, metallic MRs have been proven to efficiently produce hydrogen from SMR at lower temperatures and pressures than current industrial conditions [20–24].

Few studies exist in the literature dealing with hydrogen production in Pd and Pd-Ag MRs using *real* NG mixtures. For example, Shirasaki et al. produced pure hydrogen at a rate of 3.6 kg/h (40 m^3/h) by using planar Pd-Ag membranes with a thickness of ~ 20 μm and a NG mixture composed by 88.5% methane, 4.6% ethane, 5.4% propane, and 1.5% butane [25]. This study mainly focused on the overall principle of large-scale hydrogen production from reforming of NG via Pd-based MRs. The authors obtained an overall average energy efficiency of > 70% and a best value of 76.2% based on the HHV of pure hydrogen produced divided by the HHV of NG along with auxiliaries (i.e., air handling equipment, heat needed for the reaction, cooling loads, NG compressor, etc.). Although the MR was operated for 3310 h and was subjected to 61 thermal cycles (from start up to shut down), it provided a hydrogen purity greater than 99.99% throughout the testing. In addition, the reformer system was optimized to realize a NG conversion of 83%, with the possibility of reaching 90% [26]. In another study [27], a mixture of CH_4 at > 90 mol.% and other HCs (C2-C4) were fed into a fluidized-bed membrane reformer (FBMR) obtaining a conversion of 58.6% based on the average CH_4 equivalent of all HC species at T = 600 °C and $p_{reaction}$ = 400 kPa. The 25-μm Pd-Ag_{25} flat composite membrane deposited on porous stainless steel (PSS) used in the work produced a H_2 purity greater than 99.99% over a 395-h period. The same authors in another study illustrated a NG conversion of 81%, with a decreased of H_2 purity of 99.988% [28].

Although higher hydrocarbons are more reactive and enhance the overall H_2 production, they also increase the coke formation, which can rapidly deactivate the nickel catalyst, and decrease the membrane performance. Usually, an additional step called pre-reforming is added to the overall SMR process, which converts all the heavier hydrocarbons in CH_4, carbon oxides, H_2 and steam and it serves to avoid catalyst deactivation and to enhance heat recovery.

Therefore, the aim of this work is to use a thin Pd-Au membrane supported on PSS to perform the NG SR reaction and to evaluate how the heavier HCs and impurities, such as CO_2, present in NG may impact the Pd-Au MR performance in terms of conversion and hydrogen production. A comparison between SMR and NG SR reactions is also performed and evaluated. This paper will lay the foundation for a direct performance evaluation between different reactants, a first of its kind comparative analysis using MR technology.

2. Experimental details

2.1. Membrane fabrication and membrane reactor details

The composite Pd-Au/PSS membrane used in this work was fabricated at Worcester Polytechnic Institute's Center for Inorganic Membrane Studies. The commercial PSS support was purchased from Pall AccuSep, and it was already characterized by a deposited layer of zirconia on the outer surface. The outer diameter of the support was 1 cm and its total active length was 3.6 cm. The electroless plating was used to deposit a dense Pd layer by using a similar procedure to Ma et al. [29–31]. A thin gold layer was deposited on top of the palladium surface via conventional electroplating, which allows for obtaining films of desired thickness [32]. Notice that gold has been shown to enhance the properties of Pd-based membranes, such as permeance, stability and contaminant-recoverability [33], and therefore, it was used in this work. In addition, the optimum amount of gold is 5%, which has a negligible effect on the total cost of the membrane. Finally, to provide active sites on the asymmetric membrane, and to enhance the initial H_2 flux and decrease the overall time of annealing as shown within the literature [33], a pure Pd topmost layer was deposited.

The thickness of the membrane was estimated by gravimetric methods. Specifically, the final membrane was characterized by a Pd layer of approximately 12-μm thickness and a thin layer of 4.4 wt% Au, with a total active area of 11.3 cm^2. A photo showing the final membrane along with a schematic of the metallic layers on the PSS support is shown in Fig. 1.

One end of the membrane was welded to a 316-L nonporous-capped tube while the other end was welded to a nonporous tube. A commercial Ni-based catalyst supplied by Johnson Matthey Inc. was used. Before packing 3 g of catalyst in the annular region of the MR, it was crushed and sieved to an approximate particle size of 200–400 μm, in order to increase the available surface area for the reaction and to avoid pressure drop in the catalytic bed.

A cross-section of the MR system is shown in Fig. 2.

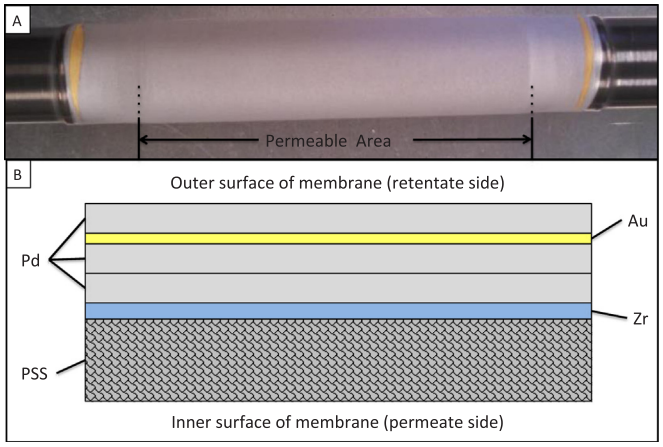

Fig. 1. Pd-Au composite membrane A) actual membrane B) schematic of membrane layers.

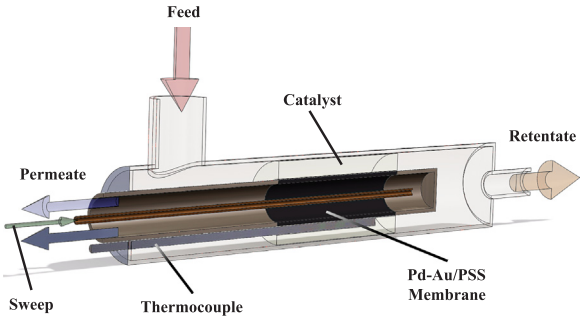

Fig. 2. Cross-section of the Pd-Au MR.

2.1.1. Experimental details

The MR system was heated using heating tape controlled by a voltage controller (Glas-Col) and the temperature was monitored via a K-type thermocouple (Omega Engineering) housed in the permeate side of the MR. Pure gases were regulated and supplied to the MR via Aalborg GFC17 thermal mass flow controllers, distilled water was supplied through an Eldex 1LMP pump, which was vaporized and mixed with gases prior to entering in the MR, a temperature-regulated water bath (Julabo F25-EH) was used to condense water vapor from the retentate and an Extrel Max-300LG Mass Spectrometer (MS) was utilized for analyzing the composition of dry gas species coming from both retentate and permeate sides. Before beginning experiments, the MS was calibrated using the standard addition method [34] in order to obtain accurate molar compositions with parts per million (ppm) precision for both retentate and permeate streams.

The MR was heated to the operating temperatures with a heating ramp of 1 °C/min under an Ar atmosphere. The effect of both NG and CH_4 feed gases on the MR performance under different reaction pressures between 100 and 300 kPa was evaluated. The reaction temperature, steam-to-methane ratio (S/CH_4), gas hourly space velocity (GHSV), and sweep gas were kept constant at 450 °C, 3.5/1, 2600 h^{-1}, and 100 mL/min, respectively.

The NG composition used in this work is reported in Table 2. Notice that the N_2 effect was already investigated by the same authors in a previous study [24]; therefore, its influence was not considered in this study.

Prior to the reaction experiments, the membrane was characterized by permeation measurements using pure gases, such as H_2 and Ar. The permeating flux of each gas through the membrane was measured using a bubble-flow meter, along with a MS, with an average of 15 experimental points recorded.

The equations used to describe the permeating characteristics of the membrane are as follows:

Table 2
Composition used for the reaction tests in this work.

Species	Composition [wt%]
Methane	86.63
Ethane	5.86
Propane	3.50
Butane	1.51
Carbon Dioxide	2.50

$$J_{H2} = P(p^{n}_{H2,\ \ retentate} - p^{n}_{H2,\ \ permeate}) \tag{16}$$

where J_{H_2} is the hydrogen permeating flux through the membrane, P is the permeance, p_{H_2} is the partial pressure of hydrogen in either the retentate or permeate side of the membrane and n is the dependent factor that relates the hydrogen partial pressure to its flux and varies between 0.5 and 1.0.

$$P = \quad P^{o} \bullet exp(-E_a/RT) \tag{17}$$

where P^o is the pre-exponential factor, E_a apparent activation energy, R universal gas constant, and T is absolute temperature.

$$\text{Ideal selectivity}\left(\alpha_{H_2/Ar}\right) = \quad \frac{Permeance_{H2}}{Permeance_{Ar}} \tag{18}$$

Each permeation point obtained represents an average value of at least 10 measurements taken over 20 min at steady-state conditions with an error variation lower than 1%.

In terms of the reaction experiments, each point obtained represents an average value of at least 100 measurements taken over 150 min at steady-state conditions with an error variation lower than 1%. The main equations used for describing the performance of the Pd-Au/PSS MR are:

$$\text{Methane conversion}\left(X_{CH_4}\right) = \frac{Q_{CH_4}{}^{IN} - Q_{CH_4}{}^{OUT}}{Q_{CH_4}{}^{IN}} \bullet 100 \tag{19}$$

$$\text{Ethane conversion}(X_{C_2H_6}) = \frac{Q_{C_2H_6}{}^{IN} - Q_{C_2H_6}{}^{OUT}}{Q_{C_2H_6}{}^{IN}} \bullet 100 \tag{20}$$

$$\text{Propane conversion}\left(X_{C_3H_8}\right) = \frac{Q_{C_3H_8}{}^{IN} - Q_{C_3H_8}{}^{OUT}}{Q_{C_3H_8}{}^{IN}} \bullet 100 \tag{21}$$

$$\text{Butane conversion}\left(X_{C_4H_{10}}\right) = \frac{Q_{C_4H_{10}}{}^{IN} - Q_{C_4H_{10}}{}^{OUT}}{Q_{C_4H_{10}}{}^{IN}} \bullet 100 \tag{22}$$

where $Q_{C_xH_y}{}^{IN}$ is the reactant flow rate entering the MR and $Q_{C_xH_y}{}^{OUT}$ is the flow rate of the unreacted species leaving the MR.

$$\text{Hydrogen recovery } (HR) = \frac{Q_{H_2}{}^{Permeate}}{Q_{H_2}{}^{Retentate} + Q_{H_2}{}^{Permeate}} \bullet 100 \tag{23}$$

$$\text{Hydrogen permeate purity } (HPP) = \frac{Q_{H_2}{}^{Permeate}}{Q_{Total}{}^{Permeate}} \bullet 100 \tag{24}$$

where $Q_{H_2}{}^{Permeate}$ and $Q_{H_2}{}^{Retentate}$ are the molar flow rates of H_2 in the permeate and retentate streams, respectively, and $Q_{Total}{}^{Permeate}$ is the total molar flow rate of the permeate stream of the membrane.

The formation of other hydrocarbons, i.e., ethylene, propylene, was not detected by the MS. Additionally, in order to evaluate whether coke formation occurs during reaction testing, pure H_2 was supplied to the MR after the experiment and the retentate stream was analyzed using the MS to check for the presence of CH_4 [35].

$$C + H_2 \leftrightarrow CH_4 \qquad \Delta H^{\circ}_{298K} = -75.0 \text{ kJ/mol} \tag{25}$$

It was found that coke was not formed in any of the experiments performed in this work. Moreover, the carbon balance between the inlet and outlet gaseous streams was closed with ± 2.0% error. Before

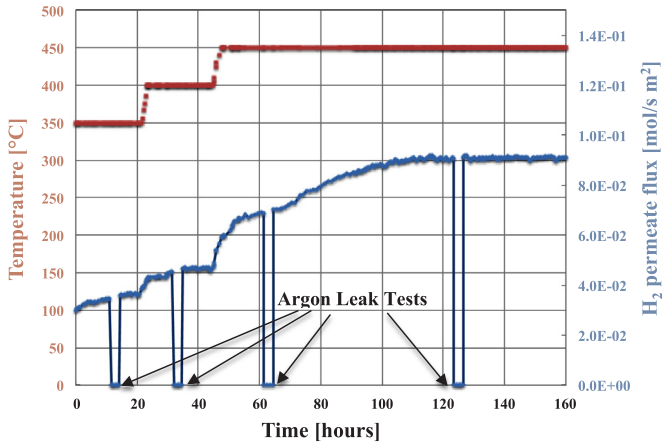

Fig. 3. Hydrogen permeating flux, argon leak tests at 350, 400, 450 °C at different elapsed times. Δp = 50 kPa.

performing the reaction experiment, the catalytic bed was reduced through the addition of hydrogen at 450 °C. The catalyst was stable throughout all of the experimental tests.

2.2. 3 Experimental results

2.2.1. Membrane annealing

The temperature of the membrane was increased from room temperature to 350 °C under an Ar environment. At this temperature and at 50 kPa of trans-membrane pressure, argon leak test showed an undetectable leak, and hydrogen was introduced to the module. The hydrogen permeating flux was measured as a function of time, continuously every 30 min, as shown in Fig. 3. Once a steady hydrogen flux was achieved at 350 °C, the temperature was increased to 400 °C and argon leak tests were performed displaying undetectable Ar leak. This procedure was repeated until a working temperature of 450 °C was reached. The temperature was kept constant at 450 °C for more than 100 h and the hydrogen permeating flux increased from 6.17×10^{-2} mol/s-m^2 to 9.15×10^{-2} mol/s-m^2. The annealing caused an increase in the hydrogen permeating flux, which led to the formation of a complete alloy of the three deposited layers of Pd-Au-Pd. This procedure allows for obtaining the maximum permeability for Pd-Au as theoretically predicted [36,37]. During this period several leak tests were performed and Ar was not detectable.

At the end of the annealing period, the membrane showed a H_2 permeance of 1.30×10^{-3} mol/s-m^2-Pa$^{0.5}$ at 450 °C. A selected summary of permeance data from different literature sources is summarized in Table 3, including the results from the current study.

It can be noted that the hydrogen permeance of the presented Pd-Au/PSS membrane is superior to the permeance of the Pd-based membranes at 450 °C, and it shows the same order of other Pd-based membranes working at higher temperature. This enhanced behavior of the membrane is due to the presence of gold, which can raise the permeance up to 2 × due to an increase in diffusivity [44,45]. Although the amount of gold in the presented membrane is 4.4%, which is just below the optimum 5% [46], the membrane displayed an excellent and stable H_2 flux.

Table 3
Selected permeance data from the literature for Pd-based membranes.

Membrane	Thickness [μm]	Temperature [°C]	Permeance [mol/s-m^2-Pa$^{0.5}$]	Reference
Pd/Al_2O_3	13	500	9.50×10^{-4}	[39]
Pd-Ag	50	450	2.00×10^{-5}	[40]
Pd/PSS	11	523	1.11×10^{-3}	[41]
Pd-alloy	15	540	2.00×10^{-3}	[42]
Pd	11	600	1.70×10^{-3}	[43]
Pd-Au/PSS	12	450	1.30×10^{-3}	This work

2.2.2. Permeation tests

Permeation tests with pure gases, such as H_2 and Ar, were carried out and ideal selectivities were evaluated at different temperatures and trans-membrane pressures of 350, 400 and 450 °C and 50, 100 and 150 kPa, respectively. In particular, permeation measurements with Ar were performed to investigate the presence of any defects within the metallic layer and were then used to calculate the ideal selectivity $\alpha_{H2/Ar}$. The membrane exhibited near-infinite selectivity at each temperature and pressure tested except for 450 °C and at pressures above 100 kPa. Specifically, at 450 °C the ideal selectivity decreased from infinity at 50 kPa to 12400 at 150 kPa. This decreasing trend can be attributed to the defects of the membrane, which are potentially caused by irregularities in the support surface and/or impurities present during electroless plating fabrication of the membrane [23]. These defects allow for Knudsen diffusion of the gas from the retentate to permeate through the defects in the Pd layer, as also reported previously by Rothenberger et al. [47]. These results indicate that the composite Pd-based membrane was not completely defect-free and not fully selective to hydrogen permeation with respect to all other gases at higher pressure than 100 kPa and 450 °C, although the H_2/Ar ideal selectivity was still high compared to the DOE H_2/N_2 ideal selectivity target of 10000.

In order to establish the membrane permeation characteristics towards hydrogen permeation, P^o, E_a and n need to be estimated. At 350 °C and 400 °C, the hydrogen permeation flux as a function of the difference in partial pressure of hydrogen to the power of n was plotted and a linear regression equation with associated R^2 was used to evaluate the n value. The best linear fit corresponding to the highest coefficient of determination, R^2, was found for $n = 0.5$ indicating that the permeation follows the Fick-Sieverts' law. At 450 °C the best linear fit corresponding to the highest coefficient of determination, R^2, was found for $n = 0.53$, as shown in Fig. 4. Therefore, at this temperature, the transport of hydrogen through the membrane is mainly limited by a solution-diffusion transport mechanism through the bulk metallic phase. Nevertheless, a deviation from 0.5 indicates that the permeation of hydrogen may be influenced by a combination of other factors such as Pd surface impurities, bulk defects, i.e., organic contaminants from fabrication or pinholes, respectively [48,49].

In order to evaluate E_a and P^o, an Arrhenius relationship between the hydrogen permeance and the reciprocal temperature was used. Values for E_a and P^o of 18.15 kJ/mol and 2.50×10^{-8} mol/s m^2 Pa were determined, respectively. These values are in reasonable agreement with other studies utilizing Pd-Au membranes, i.e., 13.1 kJ/mol for 9 wt% Au deposited on a Pd/Al_2O_3 membrane [33], as well as the range 7.9–19.2 kJ/mol for the varied composition of Au between 5 and 40 wt% [50] and a range of 11.1–18.8 kJ/mol for Pd-Au/Al_2O_3

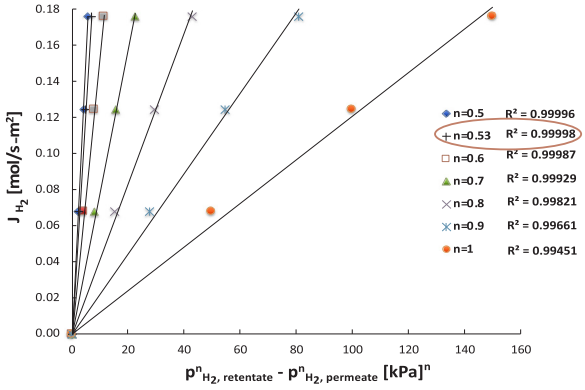

Fig. 4. H_2 flux through Pd-Au/PSS supported membrane vs the trans-membrane pressure by varying 'n' at T = 450 °C.

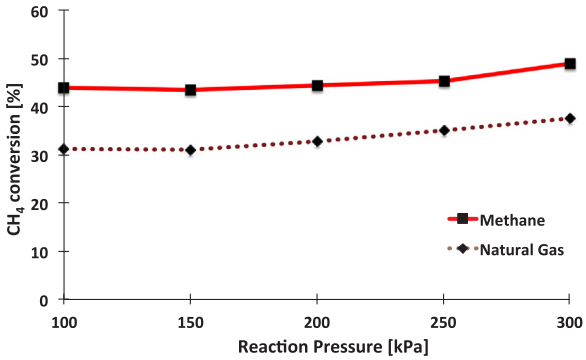

Fig. 5. Methane conversion vs reaction pressure for both pure methane and NG feeds by using Pd-Au/PSS MR at T = 450 °C, S/CH_4 = 3.5/1, GHSV = 2600 h^{-1}, $p_{permeate}$ = 100 kPa.

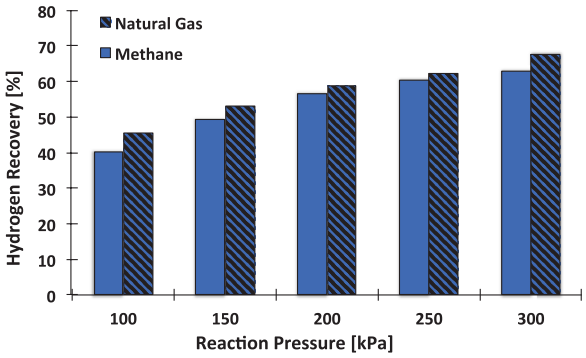

Fig. 6. HR *vs* reaction pressure for both pure methane and NG feeds by using Pd-Au/PSS MR at T = 450 °C, S/CH_4 = 3.5/1, GHSV = 2600 h^{-1}, $p_{permeate}$ = 100 kPa.

membranes [51]. In addition, the membrane showed high stability in terms of selectivity and no performance decrease for over long periods of time, i.e., > 1000 h.

2.2.3. Reaction tests

The SR reaction testing using NG mixture as a feed was performed in the Pd-Au/PSS MR at T = 450 °C, S/CH_4 = 3.5/1, GHSV = 2600 h^{-1}, and $p_{permeate}$ = 100 kPa. The MR performance in terms of CH_4 conversion, HR, and HPP was investigated at different reaction pressures and the effect of the heavier HCs was evaluated by performing the SR of methane at the same operating conditions. Fig. 5 shows the methane conversion vs the reaction pressure for both NG and methane feeds. As displayed, the methane conversion slightly increases with increasing reaction pressure for both feeds. This increasing trend is caused by a growing shift effect promoted by a higher hydrogen permeation driving force. In particular, an increase in the reaction pressure results in an increased H_2 partial pressure in the retentate stream. This causes a higher H_2 permeation flux through the membrane, thereby causing more hydrogen to be removed from the reaction zone, driving the reactions towards further product formation and resulting in an increase in the methane conversion. This phenomenon is called the 'shift effect'.

By comparing the two feeds, it is visible that the methane conversion is higher when pure methane is used with respect to NG at all tested pressures. The lower methane conversion obtained by using NG is likely due to the presence of the other HCs, which react to produce methane, Eqs. (6), (7), (12), and (13), thereby causing a lower estimate of the methane conversion. Additionally, the presence of CO_2 within the NG feed can decrease the conversion, since it is a product of the reaction [33]. The maximum methane conversion obtained by using pure methane and NG feeds was 48% and 37%, respectively at 450 °C and at 300 kPa. However, although the conversion of methane was lower at all tested pressures by feeding NG, the amount of hydrogen produced was greater.

Fig. 6 shows the HR by varying the reaction pressure for both feeds. The higher HR obtained by using a NG feed can be attributed to the presence of the HCs. Indeed, high conversion of propane, butane and ethane has been obtained at all pressures tested, as shown in Fig. 7, which has produced more hydrogen, enhancing the hydrogen permeation driving force. The higher the driving force, the higher the hydrogen permeation flux through the membrane. As a consequence, a greater amount of H_2 was collected in the permeate stream, increasing the HR value. The conversion of each HC can be found in Fig. 7. As can be seen, the conversion increases with increasing pressure due to the shift effect. The lowest and highest values of the conversion for each HC were: ethane 89.5 – 93%, propane 88.5 – 92%, and butane 76 – 83%.

In addition to the data presented in Fig. 7, the CO_2 and CO selectivities (flow rate of the respective gas divided by the total gas flow rate) for methane and NG SR reactions are shown in Fig. 8(a,b).

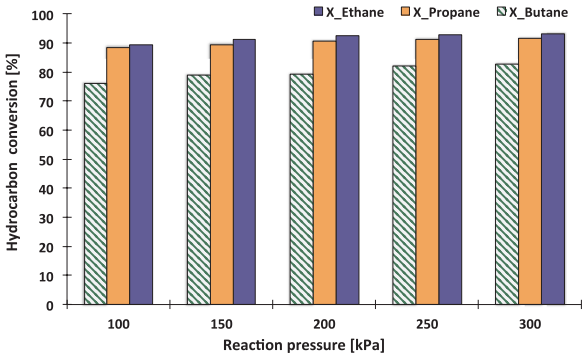

Fig. 7. HCs conversion *vs* reaction pressure for NG feed by using Pd-Au/PSS MR at T = 450 °C, S/CH_4 = 3.5/1, GHSV = 2600 h^{-1}, $p_{permeate}$ = 100 kPa.

As the reaction pressure is increased, an increasing trend in the formation of CO_2 and a decreasing trend in the formation of CO are found for both feeds. This is due to the increased permeated hydrogen flux with increasing pressure, which shifts the reactions towards further product formation, among which include CO_2, thereby resulting in a higher consumption of CO due to the WGS reaction. This effect is more evident when using an NG feed because of higher hydrogen permeation, which enhances the shift effect.

In all of the experiments carried out, the HPP was found to be approximately 100% indicating that, by using a condensable sweep gas such as steam, the hydrogen coming from the permeate stream can be used directly for industrial applications as well as a fuel cell feed. In addition, steam increases the methane conversion due to the presence of oxygen. In addition, there is no structural damage caused in the composite Pd-based membranes, as shown in the study of Gallucci et al. [52].

Also, no coke formation was detected in the entire experimental tests indicating that the MR is stable under the operating conditions used in this work and can produce high-purity hydrogen from an NG mixture to be directly used.

3. Pd-Au membrane characterization post reaction testing

The scanning electron microscope (SEM) and energy-dispersive X-ray spectroscopy (EDS) techniques were performed after the tests to characterize the Pd-Au composite membrane used in this study – primarily to verify and determine the thickness and composition. Fig. 9 shows (a) the membrane surface and (b) a cross sectional image of the supported Pd-Au membrane using SEM. From the superficial SEM image, it can be seen that the Pd-Au membrane after tests still presents the characteristic cauliflower morphology of Pd clusters indicating that the membrane did not degrade under the conditions used during the

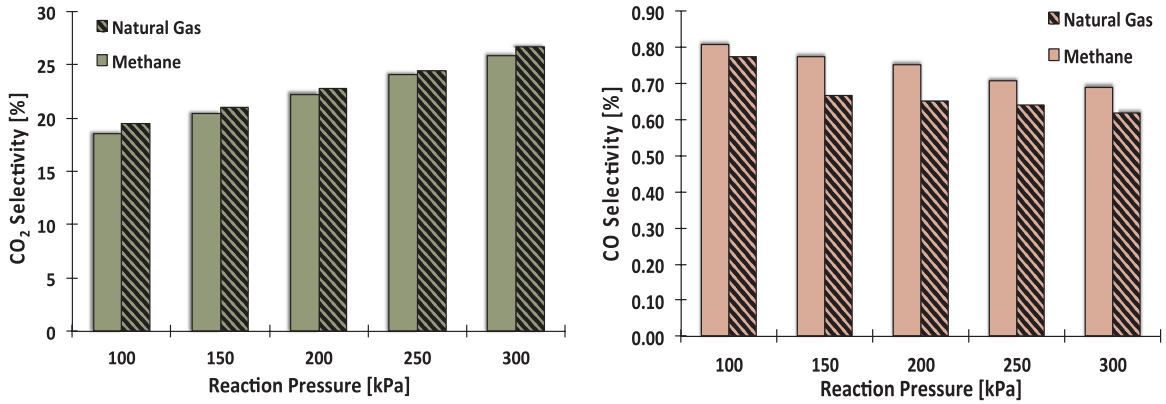

Fig. 8. a) CO_2 selectivity and b) CO selectivity *vs* reaction pressure for pure methane feed and NG feed by using Pd-Au/PSS MR at T = 450 °C, S/CH_4 = 3.5/1, GHSV = 2600 h^{-1}, $p_{permeate}$ = 100 kPa.

testing.

Regarding the cross-sectional image, the real thickness of the membrane is approximately 12 μm, although it looks bigger in EDS image. This is due to the cutting and polishing procedures of the sample that, in this case, did not offer a flat surface for the physical and chemical characterizations. Therefore, the Pd layer is affected by the 'background readiness', which magnifies the real thickness dimensions. The EDS analysis took place to understand the diffusion of dissimilar metals deposited as elemental rich layers, i.e., the Au-rich layer into the Pd-rich layers. The plating of two dissimilar layers of metal has been shown to be an effective approach for the production of a hydrogen-permeable membrane [53–55]. Several factors surrounding the use of bilayer deposition relating to lower permeation, hydrogen embrittlement, and metallic delamination of alloying have recently been overcome [56–60]. One prevailing method that has yielded good success is the deposition of hydrogen permeable layers around the alloyed metal, i.e., Pd-metal-Pd as this has shown to allow for elevated hydrogen permeation while the diffusion of dissimilar metals takes place [61–63]. Based on a literature search, the membrane used during the current work had two different electroless plated layers of Pd and one layer of electroplating of Au. Methods for achieving homogeneous metal alloys vary throughout the literature, but one common method is that annealing the alloyed membrane at an elevated temperature aids in diffusion due to the increased movement of atoms [64,65].

Fig. 10 shows the primary placement of the elements associated with the fabrication of the Pd-Au membrane. Fig. 10A shows the initial porous SS support in red, Fig. 10B has the manufacturer deposited ZrO_2 layer visible in yellow. Fig. 10C contains the as-deposited Pd layer shown in purple with a uniform thickness. Fig. 10D shows two signals in blue, the Au layer close to the upper-most part of the Pd layer of the membrane and the ZrO_2 layer close to the PSS. It is also important to note that the Au-rich layer shows some Au that has diffused through the Pd layer, but still has a high concentration in the area of original deposition.

Unfortunately, it is hard to conclude that the Au-rich layer has created a homogeneous layer with Pd, as there is not an untested membrane for comparison. What has been shown throughout this experimental work is a high H_2 permeation and high ideal selectivity, thereby leading to the conclusion that this type of fabrication can be used for NG SR reaction testing.

4. Conclusions

The results of this study have shown that the use of pipeline-sourced natural gas for the purpose of producing high-purity hydrogen is attainable at milder conditions than the conventional industrial method for producing hydrogen via SMR. Although the conversion of methane was lower when using *real* natural gas as compared to pure methane, the production of hydrogen was greater due to the high conversions of the other hydrocarbons: ethane (93%), propane (92%) and butane (83%). These results suggest that by using the MR technology with a *real* natural gas mixture, high conversions and high hydrogen recovery can be achieved at low operating temperatures (450 °C) and pressures (300 kPa). This highlights the ability of the MR to produce hydrogen at mild conditions with respect to the commercial hydrogen production process. It is also important to note that no coke was detected during the testing.

Furthermore, the Pd-Au membrane showed stability in terms of

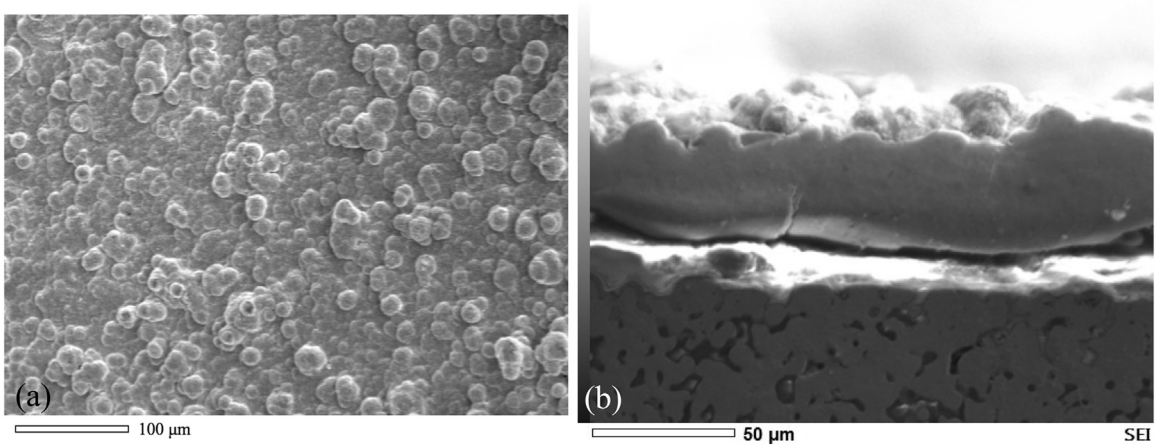

Fig. 9. SEM imaging of (a) surface (b) and cross section of the Pd-Au composite membrane.

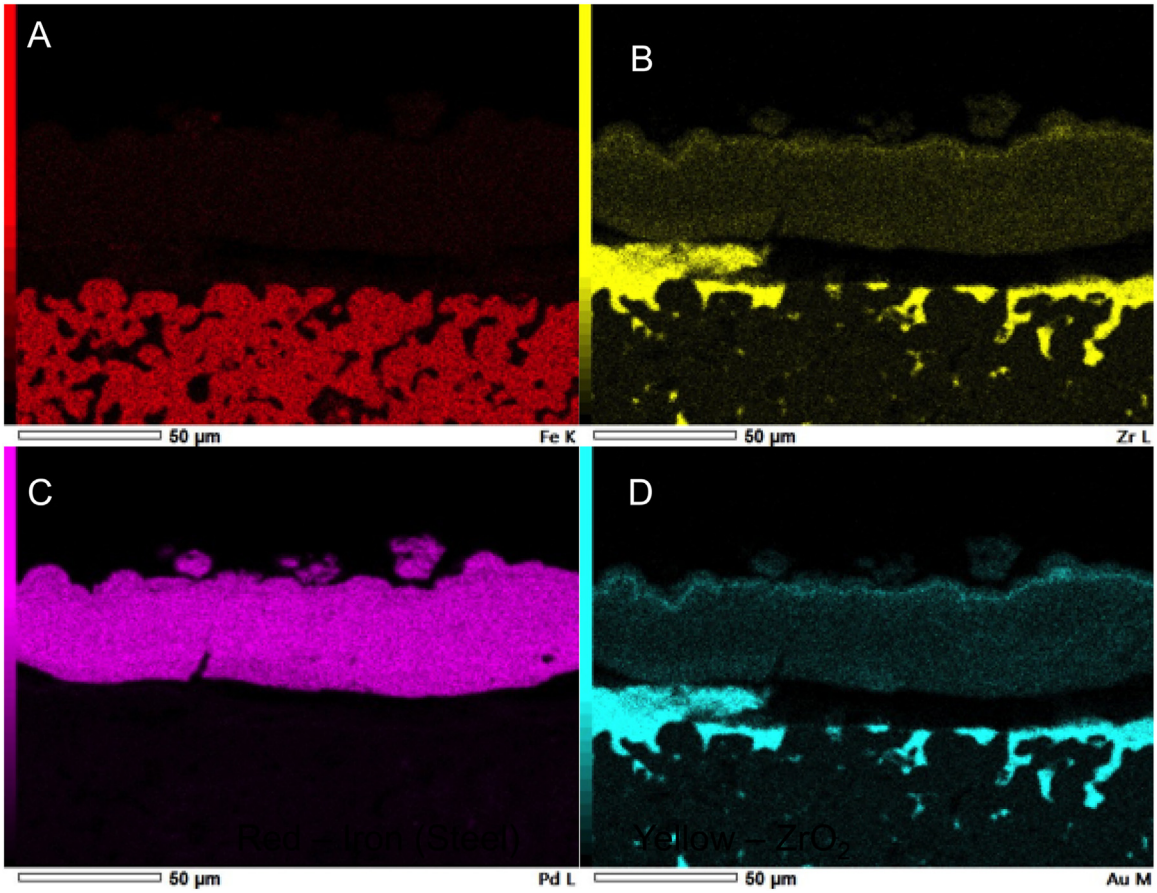

Fig. 10. Elemental analysis of Pd-Au membrane cross-section: A) Porous SS support, B) ZrO_2 intermediate layer, C) deposited Pd layer, D) Deposited Au layer.

ideal selectivity, which was near-infinite at 350 and 400 °C, with a hydrogen permeate purity of 100% for over long periods of time, i.e., > 1000 h. These results indicate that by producing a bi-layer metallic membrane through electroless plating of Pd and electroplating of Au, an established alloy is achievable for its use under steam reforming reactions. In order to understand the dynamics of using natural gas as the feed for steam reforming within the Pd-Au MR, further results will be discussed in future work.

Acknowledgements

The Stanford University School of Earth, Energy & Environmental Sciences Graduate Fellowship Program supported this work. The authors would like to thank Dr. Kyoungjin Lee for her support in the SEM images and elemental analysis used in this work.

References

[1] P. Hoffmann, Tomorrow's Energy: Hydrogen, Fuel Cells, and the Prospects for a Cleaner Planet, MIT press, 2012.
[2] C.M. Kalamaras, A.M. Efstathiou, Hydrogen Production Technologies: Current State and Future Developments, Conference Papers in Science, Hindawi Publishing Corporation, 2013.
[3] G.W. Crabtree, M.S. Dresselhaus, M.V. Buchanan, The hydrogen economy, Phys. Today 57 (2004) 39–44.
[4] U.S.E.I. Administration, Natural Gas Gross Wishdrawals and Production, in, 2016.
[5] H. Wang, I.J. Duncan, Understanding the nature of risks associated with onshore natural gas gathering pipelines, J. Loss Prev. Proc. Ind. 29 (2014) 49–55.
[6] B. Guo, A. Ghalambor, Natural Gas Engineering Handbook, Elsevier, 2014.
[7] S. Mokhatab, W.A. Poe, Handbook of Natural Gas Transmission and Processing, Gulf Professional Publishing, 2012.
[8] M.M. Foss, C. Head, Interstate Natural Gas-Quality Specifications & Interchangeability, Center for Energy Economics, Bureau of Economic Geology, University of Texas at Austin, 2004.
[9] A.L. Dicks, Hydrogen generation from natural gas for the fuel cell systems of tomorrow, J. Power Sources 61 (1996) 113–124.
[10] J.P. Van Hook, Methane-steam reforming, Catal. Rev. -Sci. Eng. 21 (1980) 1–51.
[11] J. Xu, G.F. Froment, Methane steam reforming, methanation and water-gas shift: i. Intrinsic kinetics, AIChE J. 35 (1989) 88–96.
[12] M.V. Twigg, M. Twigg, Catalyst Handbook, CSIRO, 1989.
[13] X. Huang, R. Reimert, Kinetics of steam reforming of ethane on Ni/YSZ (yttria-stabilised zirconia) catalyst, Fuel 106 (2013) 380–387.
[14] N. Laosiripojana, W. Sangtongkitcharoen, S. Assabumrungrat, Catalytic steam reforming of ethane and propane over CeO_2-doped Ni/Al_2O_3 at SOFC temperature: improvement of resistance toward carbon formation by the redox property of doping CeO_2, Fuel 85 (2006) 323–332.
[15] A.K. Avcı, D.L. Trimm, A.E. Aksoylu, Z.I. Önsan, Hydrogen production by steam reforming of n-butane over supported Ni and Pt-Ni catalysts, Appl. Catal. A: Gen. 258 (2004) 235–240.
[16] P.L. Spath, M.K. Mann, Life Cycle Assessment of Hydrogen Production via Natural Gas Steam Reforming, National Renewable Energy Laboratory, Golden, CO, 2000.
[17] J. Ross, A. Van Keulen, M. Hegarty, K. Seshan, The catalytic conversion of natural gas to useful products, Catal. Today 30 (1996) 193–199.
[18] B.C. Steele, Fuel-cell technology: running on natural gas, Nature 400 (1999) 619–621.
[19] X. Jing, Design of a promoter to enhance the stability of catalysts for hydrocarbon reactions, in, 2008.
[20] H.W.A. El Hawa, S.-T.B. Lundin, N.S. Patki, J.D. Way, Steam methane reforming in a Pd Au membrane reactor: Long-term assessment, Int. J. Hydrog. Energy 41 (2016) 10193–10201.
[21] J.A. Medrano, E. Fernandez, J. Melendez, M. Parco, D.A.P. Tanaka, M. van Sint Annaland, F. Gallucci, Pd-based metallic supported membranes: high-temperature stability and fluidized bed reactor testing, Int. J. Hydrog. Energy 41 (2016) 8706–8718.
[22] M. Patrascu, M. Sheintuch, On-site pure hydrogen production by methane steam reforming in high flux membrane reactor: experimental validation, model predictions and membrane inhibition, Chem. Eng. J. 262 (2015) 862–874.
[23] B. Anzelmo, J. Wilcox, S. Liguori, Natural gas steam reforming reaction at low temperature and pressure conditions for hydrogen production via Pd/PSS membrane reactor, J. Membr. Sci. 522 (2017) 343–350.
[24] B. Anzelmo, S. Liguori, I. Mardilovich, A. Iulianelli, Y.-H. Ma, J. Wilcox, A. Basile, Fabrication & performance study of a palladium on alumina supported membrane reactor: natural gas steam reforming, a case study, Int. J. Hydrog. Energy 43 (2018) 7713–7721.
[25] Y. Shirasaki, T. Tsuneki, Y. Ota, I. Yasuda, S. Tachibana, H. Nakajima, K. Kobayashi,

Development of membrane reformer system for highly efficient hydrogen production from natural gas, Int. J. Hydrog. Energy 34 (2009) 4482–4487.
[26] Y. Shirasaki, M. Gondaira, Y. Ohta, H. Uchida, K. Kuroda, T. Uchida, Y. Fujimoto, H. Makihara, S. Ohta, K. Kobayashi, Hydrogen producing apparatus, in, Google Patents, 1997.
[27] A. Mahecha-Botero, T. Boyd, A. Gulamhusein, J.R. Grace, C.J. Lim, Y. Shirasaki, H. Kurokawa, I. Yasuda, Catalytic reforming of natural gas for hydrogen production in a pilot fluidized-bed membrane reactor: mapping of operating and feed conditions, Int. J. Hydrog. Energy 36 (2011) 10727–10736.
[28] A. Mahecha-Botero, T. Boyd, A. Gulamhusein, N. Comyn, C.J. Lim, J.R. Grace, Y. Shirasaki, I. Yasuda, Pure hydrogen generation in a fluidized-bed membrane reactor: experimental findings, Chem. Eng. Sci. 63 (2008) 2752–2762.
[29] Y.H. Ma, I.P. Mardilovich, Composite structures with porous anodic oxide layers and methods of fabrication, in, Google Patents, 2013.
[30] Y.H. Ma, I.P. Mardilovich, E.E. Engwall, Composite gas separation modules having high Tamman temperature intermediate layers, in, Google Patents, 2007.
[31] Y.H. Ma, P.P. Mardilovich, Y. She, Hydrogen gas-extraction module and method of fabrication, in, Google Patents, 2000.
[32] S. Yun, S.T. Oyama, Correlations in palladium membranes for hydrogen separation: a review, J. Membr. Sci. 375 (2011) 28–45.
[33] C.-H. Chen, Y.H. Ma, The effect of H_2S on the performance of Pd and Pd/Au composite membrane, J. Membr. Sci. 362 (2010) 535–544.
[34] B.E. Saxberg, B.R. Kowalski, Generalized standard addition method, Anal. Chem. 51 (1979) 1031–1038.
[35] L. García, Hydrogen production by steam reforming of natural gas and other non-renewable feedstocks, Compend. Hydrog. Energy.: Hydrog. Prod. Purif. 1 (2015) 83.
[36] T.B. Flanagan, D. Wang, Hydrogen permeation through fcc Pd–Au alloy membranes, J. Phys. Chem. C 115 (2011) 11618–11623.
[37] C.G. Sonwane, J. Wilcox, Y.H. Ma, Achieving optimum hydrogen permeability in PdAg and PdAu alloys, J. Chem. Phys. 125 (2006) 184714.
[39] S. Uemiya, N. Sato, H. Ando, T. Matsuda, E. Kikuchi, Promotion of methane steam reforming by use of palladium membrane, J. Jpn Pet. Inst. 33 (1990) 418–421.
[40] F. Gallucci, L. Paturzo, A. Fama, A. Basile, Experimental study of the methane steam reforming reaction in a dense Pd/Ag membrane reactor, Ind. Eng. Chem. Res. 43 (2004) 928–933.
[41] J. Tong, Y. Matsumura, Effect of catalytic activity on methane steam reforming in hydrogen-permeable membrane reactor, Appl. Catal. 286 (2005) 226–231.
[42] Y. Shirasaki, T. Tsuneki, Y. Ota, I. Yasuda, S. Tachibana, H. Nakajima, Development of membrane reformer system for highly efficient hydrogen production from natural gas, Int. J. Hydrog. Energy 34 (2009) 4482–4487.
[43] B. Dittmar, A. Behrens, N. Schödel, M. Rüttinger, T. Franco, G. Straczewski, Methane steam reforming operation and thermal stability of new porous metal supported tubular palladium composite membranes, Int. J. Hydrog. Energy 38 (2013) 8759–8771.
[44] F. Guazzone, J. Catalano, I.P. Mardilovich, J. Kniep, S. Pande, T. Wu, R.C. Lambrecht, S. Datta, N.K. Kazantzis, Y.H. Ma, Gas permeation field tests of composite Pd and Pd-Au membranes in actual coal derived syngas atmosphere, Int. J. Hydrog. Energy 19 (2012) 14557–14568.
[45] D.L. McKinley, W.V. Nitro, Method for Hydrogen Separation and Purification. U.S. Patent 3,247,648, 26 April, 1966.
[46] V. Gryaznov, Metal containing membranes for the production of ultrapure hydrogen and the recovery of hydrogen isotopes, Sep. Purif. Methods 29 (2000) 171–187.
[47] K.S. Rothenberger, A.V. Cugini, B.H. Howard, R.P. Killmeyer, M.V. Ciocco, B.D. Morreale, R.M. Enick, F. Bustamante, I.P. Mardilovich, Y.H. Ma, High pressure hydrogen permeance of porous stainless steel coated with a thin palladium film via electroless plating, J. Membr. Sci. 244 (2004) 55–68.
[48] F. Guazzone, E.E. Engwall, Y.H. Ma, Effects of surface activity, defects and mass transfer on hydrogen permeance and n-value in composite palladium-porous stainless steel membranes, Catal. Today 118 (2006) 24–31.
[49] S. Paglieri, J. Way, Innovations in palladium membrane research, Sep. Purif. Methods 31 (2002) 1–169.
[50] K.G. Sabina, E.C. Kent, J.D. Way, Effects of fabrication technique upon material properties and permeation characteristics of palladium-gold alloy membranes for hydrogen separations, Gold. Bull. 43 (2010) 287–297.
[51] H. Jia, P. Wu, G. Zeng, E. Salas-Colera, A. Serrano, G.R. Castro, H. Xu, C. Sun, A. Goldbach, High-temperature stability of Pd alloy membranes containing Cu and Au, J. Membr. Sci. 544 (2017) 151–160.
[52] F. Gallucci, L. Paturzo, A. Famà, A. Basile, Experimental study of the methane steam reforming reaction in a dense Pd/Ag membrane reactor, Ind. Eng. Chem. Res. 43 (2004) 928–933.
[53] D. Baudrand, J. Bengston, Electroless plating processes: developing technologies for electroless nickel, palladium, and gold, Metal. Finish. 93 (1995) 55–57.
[54] N. Zotov, A. Ludwig, Atomic mechanisms of interdiffusion in metallic multilayers, Mat. Sci. Eng.: C 27 (2007) 1470–1474.
[55] Ø. Hatlevik, S.K. Gade, M.K. Keeling, P.M. Thoen, A. Davidson, J.D. Way, Palladium and palladium alloy membranes for hydrogen separation and production: history, fabrication strategies, and current performance, Sep. Purif. Technol. 73 (2010) 59–64.
[56] A. Suzuki, H. Yukawa, T. Nambu, Y. Matsumoto, Y. Murata, Analysis of pressure–composition–isotherms for design of non-Pd-based alloy membranes with high hydrogen permeability and strong resistance to hydrogen embrittlement, J. Membr. Sci. 503 (2016) 110–115.
[57] V. Alimov, A. Busnyuk, M. Notkin, A. Livshits, Pd–V–Pd composite membranes: hydrogen transport in a wide pressure range and mechanical stability, J. Membr. Sci. 457 (2014) 103–112.
[58] F. Li, B. Zhong, H. Xiao, X. Ye, L. Lu, W. Guan, Y. Zhang, X. Wang, Ca Chen, Effect of degassing treatment on the deuterium permeability of Pd-Nb-Pd composite membranes during deuterium permeation, Sep. Purif. Technol. 190 (2018) 136–142.
[59] R. Ruhela, A. Singh, B. Tomar, R. Hubli, Separation of palladium from high level liquid waste–a review, RSC Adv. 4 (2014) 24344–24350.
[60] E. Legrand, Numerical Approach of the Scale Transitions Applied to the Diffusion and the Trapping of Hydrogen in Metals With Heterogeneous Structures, Université de La Rochelle, 2013.
[61] D.J. Edlund, J. McCarthy, The relationship between intermetallic diffusion and flux decline in composite-metal membranes: implications for achieving long membrane lifetime, J. Membr. Sci. 107 (1995) 147–153.
[62] L.N. Baloyi, B.C. North, H.W. Langmi, B.J. Bladergroen, T.V. Ojumu, The production of hydrogen through the use of a 77 wt% Pd 23 wt% Ag membrane water gas shift reactor, South Afr. J. Chem. Eng. 22 (2016) 44–54.
[63] W.-S. Ko, B.-J. Lee, Modified embedded-atom method interatomic potentials for pure Y and the V–Pd–Y ternary system, Model. Simul. Mater. Sci. Eng. 21 (2013) 085008.
[64] E. Fernandez, J.A. Medrano, J. Melendez, M. Parco, J.L. Viviente, M. van Sint Annaland, F. Gallucci, D.P. Tanaka, Preparation and characterization of metallic supported thin Pd–Ag membranes for hydrogen separation, Chem. Eng. J. 305 (2016) 182–190.
[65] J. Shu, A. Adnot, B. Grandjean, S. Kaliaguine, Structurally stable composite Pd- Ag alloy membranes: introduction of a diffusion barrier, Thin Solid Films 286 (1996) 72–79.